Carbon 107 (2016) 190–197

Contents lists available at ScienceDirect

Carbon

journal homepage: www.elsevier.com/locate/carbon

Chemically specific identification of carbon in XPS imaging using Multivariate Auger Feature Imaging (MAFI)

Anders J. Barlow [a, *], Sinziana Popescu [b], Kateryna Artyushkova [c], Oliver Scott [b], Naoko Sano [a], John Hedley [b], Peter J. Cumpson [a]

[a] National EPSRC XPS Users' Service (NEXUS), School of Mechanical and Systems Engineering, Newcastle University, Newcastle upon Tyne, Tyne and Wear, NE1 7RU, United Kingdom
[b] School of Mechanical and Systems Engineering, Newcastle University, Newcastle upon Tyne, Tyne and Wear, NE1 7RU, United Kingdom
[c] Department of Chemical and Biological Engineering, University of New Mexico, Albuquerque, NM, 87131, United States

ARTICLE INFO

Article history:
Received 25 March 2016
Received in revised form
6 May 2016
Accepted 30 May 2016
Available online 30 May 2016

ABSTRACT

Until now, a difficult prospect in XPS imaging has been the identification of similar chemical states of carbon. With the advent of novel nano-carbons such as nanotubes and graphene, the ability to easily and unambiguously identify materials of varying sp^2/sp^3 nature in XPS spectra and images is becoming increasingly important. We present herein methods for the identification of such species in XPS images by shifting focus from the traditionally analysed C1s region to the X-ray induced carbon Auger feature. By extracting the D-Parameter from XPS data, we have generated what we refer to as "D-Parameter Images", that clearly identify regions of different carbon hybridisation in an image of a graphite flake mounted on carbon tape, and areas of reduced graphene oxide (GO) in a laser-scribed GO film. This method is then enhanced by multivariate analysis, a technique we call "Multivariate Auger Feature Imaging", where the distinction between varying sp^2 carbon content on a surface is improved.

© 2016 The Authors. Published by Elsevier Ltd. This is an open access article under the CC BY license (http://creativecommons.org/licenses/by/4.0/).

1. Introduction

Surface analysis by X-ray photoelectron spectroscopy (XPS) is well-suited to the characterisation of carbon-based nanomaterials and films, and is a complementary technique to optical spectroscopy (Raman, IR, UV–Vis), or scanning electron/ion and scanning probe microscopies [1]. There are many allotropes of carbon and one of particular technological interest currently is that of graphene, often produced as graphene oxide through chemical or mechanical exfoliation of graphite [2].

At our multi-user facility, we provide access to state-of-the-art XPS instrumentation to academia, but also perform our own in-house research developing new and existing XPS techniques and methodologies [3–7]. One question that is often asked by our collaborators working with carbon materials is: "can we determine how much oxygen is present in a graphene oxide sample and what the ratio of sp^2 to sp^3 hybridised carbon is in the sample?". The former part of the question can be answered through the analysis of the O1s and C1s peak areas, with further peak-fitting of these regions to determine the chemical states present. In the latter case, discerning whether the carbon present in a given sample is sp^2 or sp^3 hybridised can prove to be quite difficult. While there are differences in C1s spectra between, for example, diamond and graphite (i.e. effectively pure sp^3 and sp^2 carbon respectively), these differences tend to be quite subtle, and are sometimes convoluted with extra chemical states (such as oxidation) or made difficult to elucidate due to charging effects brought on by the technique itself.

Often ignored in typical XPS analysis are the X-ray-induced Auger features. For carbon this feature is present around 260 eV (kinetic energy, KE), and arises from the relaxation and subsequent ejection of valence electrons from a carbon atom after the initial photo-ionisation by X-rays (denoted C *KLL*). Fig. 1(a) presents C1s spectra collected from a sample of graphite and of low-density polyethylene (LDPE), while Fig. 1(b) shows the corresponding C *KLL* spectra. It has previously been shown that the shape of the C *KLL* feature changes depending on the arrangement of carbon atoms in the surface under analysis [8]. These variations are elucidated through differentiation of the spectra, shown in Fig. 1(c), where the difference in energy between the maximum and minimum of the resultant curves varies considerably when going from

* Corresponding author.
E-mail address: anders.barlow@newcastle.ac.uk (A.J. Barlow).

http://dx.doi.org/10.1016/j.carbon.2016.05.073
0008-6223/© 2016 The Authors. Published by Elsevier Ltd. This is an open access article under the CC BY license (http://creativecommons.org/licenses/by/4.0/).

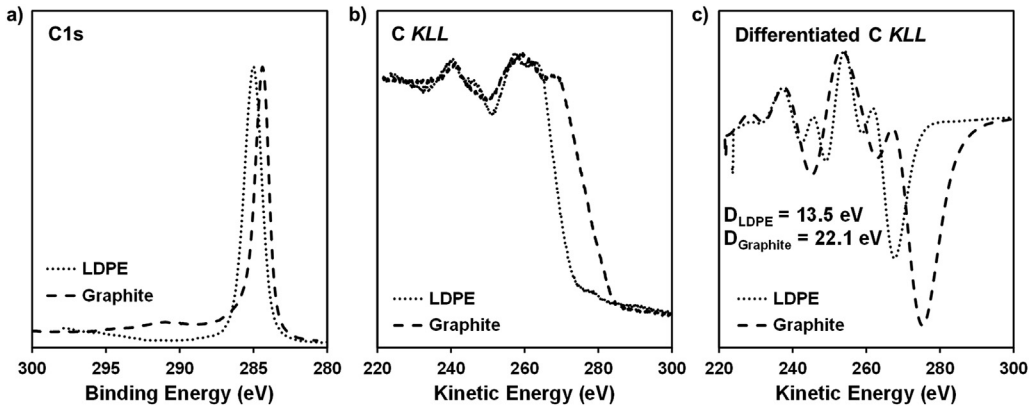

Fig. 1. LDPE and Graphite XPS spectra from a) the C1s region and b) the X-ray induced C *KLL* Auger feature. The Auger feature can be differentiated to produce the curves in c) where the difference between LDPE and Graphite is emphasised.

sp^2 to sp^3 hybridisation. This difference is commonly known as the D-Parameter, and values typically range from 11 to 13 eV for very sp^3-like materials to 21–23 eV for very sp^2-like materials [9]. The D-Parameter values for the graphite and LDPE measured here were found to be 22.1 eV and 13.5 eV respectively as measured from the AXIS Nova instrument. Table 1 provides the calculated D-Parameter values measured from the same reference samples using all three instruments in this study for comparison. Lascovich et al. presented data collected from a variety of materials that resulted in an apparently linear relationship between the estimated percentage of sp^2 carbon in samples and the measured D-Parameter [10]. Thus measurement of the D-Parameter can give analysts insight into how much of each bonding type is present in a carbon-based material in a manner that may be much easier to interpret relative to peak-fitting C1s spectra. Furthermore, since the measurement looks at the *width* of the Auger feature, and not its position, this technique is independent of sample charging, making the measurement more robust under scrutiny.

Though the spatial resolution of modern XPS instruments is quite modest compared to other similar surface analysis techniques, XPS imaging/mapping can be useful to identify regions of differing chemical structure in a sample surface, with a spatial resolution on the order of 1–10 μm. It is useful here to define what is meant by "imaging" and "mapping". Parallel XPS *imaging* collects the intensity of the signal from a specific kinetic energy related to a single elemental species across a two-dimensional field-of-view, typically hundreds of microns, and projects this image onto a 2-dimensional detector such as the delay-line detector (DLD). In parallel XPS imaging, high intensity at a given kinetic energy ideally indicates a higher proportion of that element present in that area. This can be useful for elements that have well-separated and intense photoelectron peaks in XPS spectra, such as carbon and oxygen for example which are separated by ~250 eV. This technique is sensitive to background intensity variations, and thus "background" images also need to be collected and subtracted from the elemental image. Elemental images may then tell the analyst where carbon and oxygen signals come from within the field of view, but not about the details of their chemical state. This information would have to come from further analysis utilising small-area spectroscopy. Chemical state imaging takes a similar approach, however, focuses on a single elemental region in the XPS spectrum with a narrow energy window. Contrast in this technique then comes from differences in chemical state features within a given elemental region. This can be further built-upon by collecting images at regular energy intervals across a spectral region of interest, and then combining them in post-processing (sometimes referred to as 'spectra from images'). At each pixel a spectrum can be extracted that details the chemical nature of the region of the surface around that pixel. Again, this can be a useful method, however due to the relatively high pass energy typically used in XPS imaging (and thus low spectral resolution) it still relies on features being well-separated and distinguishable from one-another.

Table 1
Measured D-Parameter values (in eV) from samples of LDPE (sp^3 carbon reference) and Graphite (sp^2 carbon reference) for the three XPS instruments used in this study.

Instrument	LDPE	Graphite
AXIS Nova	13.5	22.1
K-Alpha	13.6	21.6
Theta Probe	13.6	21.2

XPS elemental/chemical *mapping*, on the other hand, is simpler to discuss. The X-ray source and analyser are configured to give the smallest analysed area for the instrument, whether by a micro-focussed X-ray spot, or inserting apertures and choosing specific lens modes to reduce the acceptance area of the analyser. The sample position is then iterated in steps across a defined grid of points, with spectra of interest collected at each position and combined in-software to produce an intensity map. This technique has the advantage of not requiring post-processing to extract spectra, although it is likely that the achievable spatial resolution would not be as attractive compared to the parallel imaging technique.

Chemical state imaging of carbon surfaces where the prominent chemical difference is the hybridisation of the carbon species is thus a difficult prospect, since these spectra typically have very subtle differences. Fig. 2 shows an optical microscope image (taken from within our instrument) of a small graphite flake mounted on carbon tape in preparation for XPS analysis. Small area spectroscopy was performed at the regions indicated in the figure ($100 \times 100\ \mu m^2$, 20 eV pass energy), and showed very similar C1s spectra in both regions. This could suggest that there is some overlap in the analysed regions, or that indeed the flake and the tape have very similar chemical structure at their very surface. In either case, the results are somewhat ambiguous.

Recently, we published work describing a new method for resolving this ambiguity that combines the specificity of the D-Parameter measurement, with the spatial information of Parallel XPS Imaging. We called this technique Multivariate Auger Feature Imaging (MAFI) [6]. From this, XPS images could be extracted that plot the D-Parameter as a function of position, rather than simple

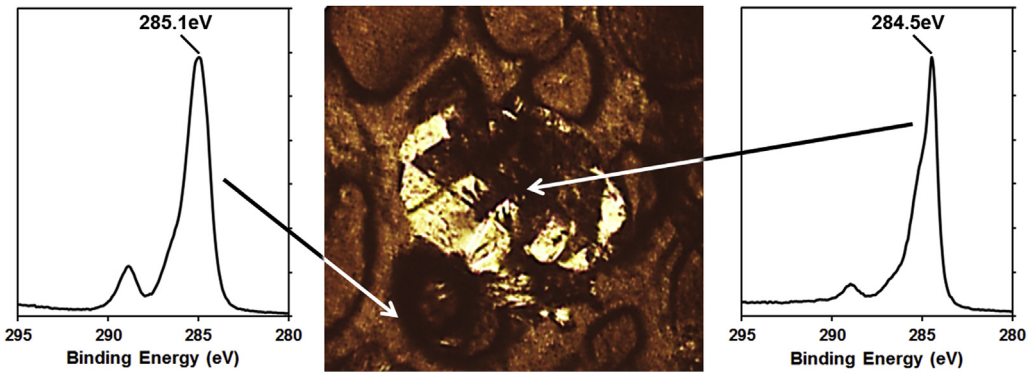

Fig. 2. Optical image of a graphite flake mounted on carbon tape. Small area spectroscopy from the regions indicated show the very similar C1s spectra for the flake and the tape, which can be problematic for XPS imaging. (A colour version of this figure can be viewed online.)

peak intensities, thereby giving the analyst an immediate and unambiguous view of the spatial distribution of the sp^2 and sp^3 content on a given sample surface. Here we discuss this method in more detail and provide a further example of its application, not only utilising XPS imaging, but also XPS mapping on a larger scale showing the chemical distribution of sp^2 carbon on a laser-scribed graphene/graphite oxide film.

2. Experimental

Parallel XPS images were collected on an AXIS Nova (Kratos Analytical, Manchester, UK) using monochromatic Al Kα radiation operating at 225 W. Images were collected using Field of View 1 (800 × 800 μm^2) with the low resolution imaging iris. Pass energy was 80 eV, and the energy interval between images was 2 eV. Data was converted to VAMAS format and processed using a combination of CasaXPS [11] (version 2.3.17) and Octave [12] (version 3.8.2). XPS mapping was performed on K-Alpha and Theta Probe XPS instruments (Thermo Scientific, East Grinstead, UK), using monochromatic Al Kα radiation operating at a maximum power of 36 W, micro-focussed to a spot size of 50–100 μm. The large-area map was collected with a stage step size of 200 μm, and a defined area of 25 × 29 points (approx. 4.75 × 5.64 mm^2), while the small-area map was collected with a step size of 50 μm and a defined area of 18 × 15 points (approx. 0.91 × 0.74 mm^2). Spectra were collected at each pixel with pass energy 40 eV and energy step size of 0.5 eV for C *KLL* spectra, and pass energy 20 eV and energy step size of 0.1 eV for C1s spectra.

LDPE film of thickness 0.125 mm was purchased from Goodfellow (Cambridge, UK, catalogue number ET311250). Graphite foil of thickness 0.20 mm (99.8% purity) was purchased from Advent Research Materials (Oxford, UK, catalogue number C117915).

Raman spectra were acquired using an Alpha 300R confocal Raman microscope (WITec Instruments, Germany) with 532 nm laser using a 100× aperture. A 100 × 100 μm^2 area was selected for acquiring multispectral Raman images using a 20× objective. Linear backgrounds were subtracted from each spectrum. Multivariate curve resolution (MCR) was applied in Matlab 2014b in PLS_Toolbox 7.9 using non-negativity constraints in both spectral and image dimensions.

3. Chemical state imaging of graphite on carbon tape

3.1. D-Parameter Imaging

We have combined the chemical specificity of the D-Parameter measurement with the spatial details afforded from parallel XPS imaging on our AXIS Nova instrument. We call this method simply "D-Parameter Imaging". XPS images are collected at regular energy intervals across the C *KLL* feature (in this case in 2 eV energy steps). This series of XPS images is then exported to the standard VAMAS format for post processing. Code written and executed in Octave then compiles these images, extracts the Auger spectrum at each pixel, processes the spectrum to obtain the D-Parameter, and constructs an image based on this value and its original *x*/*y* coordinate position in the 128 × 128 pixel image. Fig. 3 presents the end result for this analysis where the D-Parameter image is presented as a thermal map. The 'cool' colours represent regions where the D-Parameter was low, while the 'hot' colours represent regions where the D-Parameter was high. Comparing the original optical image with the generated D-Parameter Image, one can see immediately that the graphite flake is clearly distinguished from the carbon tape by a region of high D-Parameter, i.e. an area in the image related to mostly sp^2 carbon in the analysed area of the sample.

The spectra that resulted in the D-Parameter image in Fig. 3 can be extracted from the data as seen in Fig. 4(a). At the centre of the feature the C *KLL* spectrum is broad, with a width of around 20 eV, as would be expected for graphite and sp^2-like carbon, while away from the feature the spectrum is much narrower, leading to a lower D-Parameter of around 16 eV indicative of sp^3-like carbon, as one might expect for the polymeric make-up of carbon tape. The spectra are quite noisy however, an unfortunate consequence of the generally low signal of the parallel XPS imaging technique, and the already low intensity of the X-ray induced carbon Auger feature. The signal-to-noise ratio (SNR) can be improved by "binning-down" the original XPS images, i.e. taking a 128 × 128 pixel image and summing intensities from neighbouring pixels. The data was reduced to 32 × 32 pixel images, and then processed using the same Octave code, with the resulting D-Parameter image presented in Fig. 4(b). The sacrifice in spatial resolution of the image allows gains to be made in SNR for the C *KLL* spectra.

3.2. Multivariate Auger Feature Imaging (MAFI)

Multivariate analysis can be used to greatly improve data quality when applied to both XPS spectra and images [13–15]. To improve the quality of the C *KLL* spectra and thus the resulting D-Parameter image without losing spatial resolution, multivariate analysis was used to "de-noise" the original spectra using target factor analysis (TFA, performed in CasaXPS), effectively identifying the strongest factors that influence the shape of the Auger spectra, and discarding the rest of the data (i.e. discarding the noise). Once the complete set of TFA processed spectra are generated, these are used in the original image processing method to extract the D-Parameter at

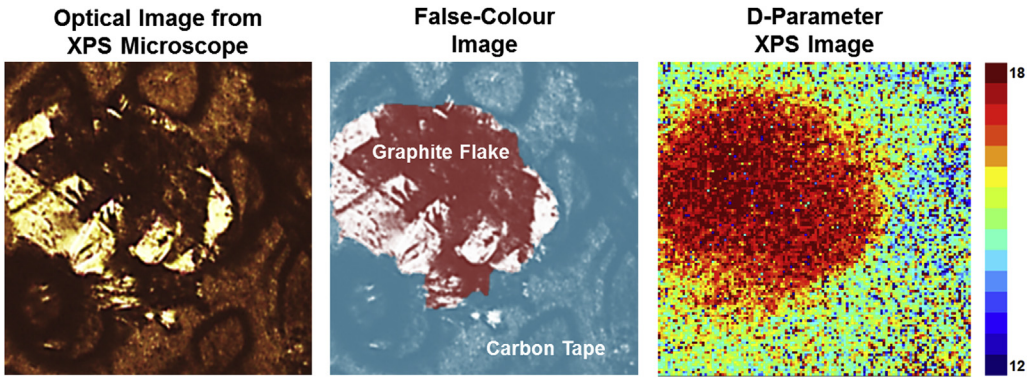

Fig. 3. D-Parameter Imaging result from graphite flake mounted on carbon tape. An optical image from within the XPS image shows the defined analysis area, with a false-colour version to highlight the graphite flake on the tape. The resulting D-Parameter image is a thermal map where 'hot' colours indicate regions of high D-Parameter, i.e. sp^2-like carbon, and 'cool' colours indicate regions of low D-Parameter, i.e. sp^3-like carbon. (A colour version of this figure can be viewed online.)

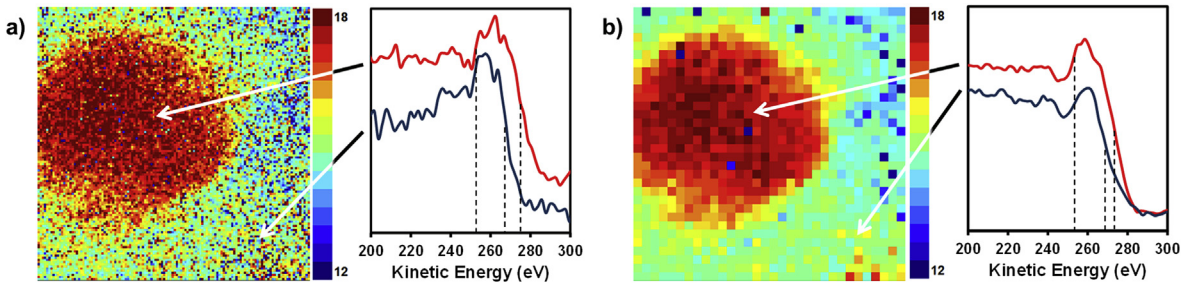

Fig. 4. D-Parameter images with C *KLL* spectra extracted from pixel resolutions of a) 128 × 128 and b) 32 × 32 pixels. Dashed lines are a guide for the width of each C *KLL* features, highlighting the greater width of the spectra from within the graphite flake region. Reducing the number of pixels enhances the signal-to-noise ratio of the spectra used in the D-Parameter analysis, but results in a lower resolution D-Parameter image. (A colour version of this figure can be viewed online.)

each pixel and generate the image. We call this "Multivariate Auger Feature Imaging" or MAFI [6], and the result is shown in Fig. 5(a). Upon removal of the noise from the C *KLL* spectra, the calculations of D-Parameter have much less scatter, and are less prone to error. Consequently, the generated image is sharper since the full 128 × 128 pixel image set can be used. As previously discussed, spectra can be extracted from the image where the improved SNR is clearly evident as shown in Fig. 5(b). Once generated, the image can be processed just like any other spectroscopic or scanned probe image using any tools readily available to the analyst. To demonstrate, we have applied a simple line-scan across the image in Fig. 5(a) as indicated by the dashed line, and plot the resulting change in D-Parameter with distance down the field of view of the image (800 × 800 μm^2) as a linescan in Fig. 5(c) as the black line. The change in D-Parameter across the graphite flake then becomes very clear, and even measurements of the dimensions of the flake could be made from such an image. Also presented in this plot is the equivalent linescan from the image in Fig. 4(a), shown as the grey line, where the extreme variability of the calculated D-Parameter due to experimental noise is evident. It is interesting to note here the surprisingly low D-Parameter value across the graphite flake. One should expect that graphite would have a value greater than 20 eV, yet the measured value here is around 17 eV. Recall Fig. 2 where we show small-spot spectra from the tape and the flake.

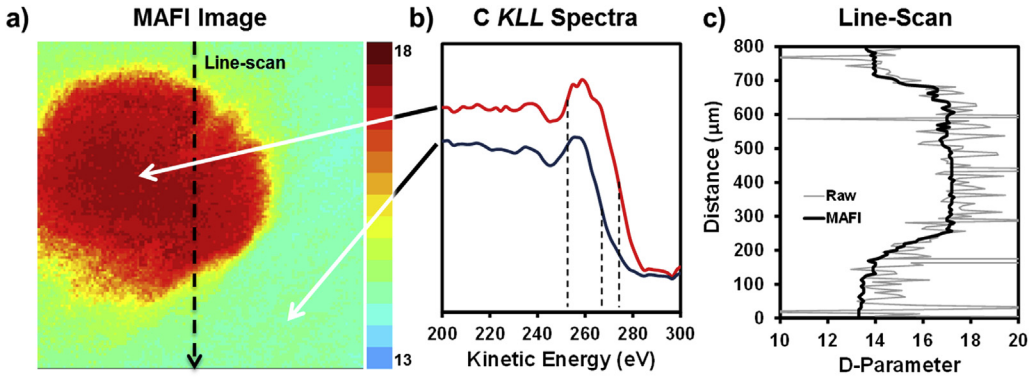

Fig. 5. (a) Multivariate Auger Feature Image of the graphite flake on carbon tape. (b) Spectra extracted from the image have higher data quality due to the TFA, and the resulting improvement in the image quality allows further analysis to be applied, such as (c) a line-scan across the feature showing the change in D-Parameter. The black line is from the MAFI image in (a), the grey line is the equivalent data from the unprocessed image in Fig. 4(a). (A colour version of this figure can be viewed online.)

The C1s peak clearly shows the presence of extra chemical states of carbon, likely associated with carbon-oxygen functionality. This would suggest that the graphite flake is not pristine in chemical functionality.

4. MAFI analysis of laser-scribed graphene oxide films

Over the last decade graphene has received a remarkable amount of research attention, owing to exceptional mechanical and electrical properties offered by the material [2,16]. Much of this research is focused on methods of graphene production, which can be broadly split into two categories; 'top-down' and 'bottom-up'. The former approach, which encompasses methods such as mechanical cleavage and chemical exfoliation, offers cost-effective production suitable for up-scaling, but is limited in control over the resulting graphene properties. The latter includes chemical vapour deposition and epitaxial growth, providing good control over the number of layers and deposition thickness, but at greater cost [17–20]. While the most pristine forms, i.e. defect and chemical functionality free, of graphene may find ultimate applications in nano-scale electronics and mechanics, graphene with some amount of defective/functionalised regions can be utilised in sensing and optical applications. Graphene/graphite oxide (GO) is commercial available in reasonable quantities, and can be processed to produce reduced graphene oxide (rGO), that while still maintaining a certain level of defects and functionality (typically carboxyl/hydroxyl), restores some of desirable properties of pristine graphene that can be harnessed in applications.

One method for the reduction of GO to rGO is that of the photothermal process via laser reduction described by El-Kady and Kaner [21]. In the present work, graphene oxide (Graphene Supermarket, USA) was diluted to 2 g/L in deionised water and ultrasonicated at room temperature for 1 h in order to ensure a good dispersion of the GO flakes. The GO was then drop-cast (15 mL) onto acetate coated discs (cut to size) and allowed to dry overnight. Once dried, the disc was loaded into a DVD writer and laser-scribed with predefined patterns (LightScribe Template Labeler software). The labelling process was repeated 6 times, obtaining well defined and dark-colour patterns for the rGO areas.

Fig. 6(a) provides a photograph of one pattern generated by the laser-scribing method; an image of the Newcastle University shield where the dark areas are the laser-scribed GO, and the light areas are the as-deposited GO. The pattern in total is approximately 5 mm × 6 mm (W × H). XPS mapping was utilised to elucidate the elemental variations in carbon and oxygen across the laser-scribed pattern. Fig. 6(b) and (c) shows the resulting quantified atomic percentage XPS maps from the K-Alpha XPS instrument using a 100 μm X-ray spot with a 200 μm step size between pixels. Maps are interpolated up to an equivalent 256 × 256 pixel density using the Avantage software (Thermo Scientific, East Grinstead, UK). By decreasing the X-ray spot size and step size to 50 μm, a smaller area could be mapped on the surface with higher spatial resolution as presented in Fig. 6(d) and (e) for C1s and O1s atomic percentages respectively. The four maps presented alongside the optical image very clearly show the relationship between carbon and oxygen content from the XPS spectra and the light and dark, i.e. as-deposited and laser-scribed, areas on the pattern. Where the laser has irradiated the deposited GO film (dark areas in Fig. 6(a)), there is a marked decrease in oxygen content as indicated by lower intensity of the O1s atomic percentage in the maps. This corresponds to an increase in the C1s atomic percentage as the two quantities are inter-dependent, and only C1s and O1s signals were detected in significant amounts on the GO films (see Supp. Info. Fig. S1).

The change in oxygen content at the surface of the laser-scribed GO compared to the as-deposited GO is unambiguous from the XPS maps. However to suggest that one has generated *reduced* GO from the deposited film would require evidence suggesting the defective sp^3-like features of the GO platelets are reduced under laser irradiation, and that the loss of oxygen relates to an increase in the sp^2 carbon content of the surface.

Results from the analysis of the surfaces in confocal Raman microscopy are given in Fig. 7. Fig. 7(a) shows the optical image of the central "cross" feature of the sample. As before, the dark areas are those that were scribed by the laser, and thus are expected to

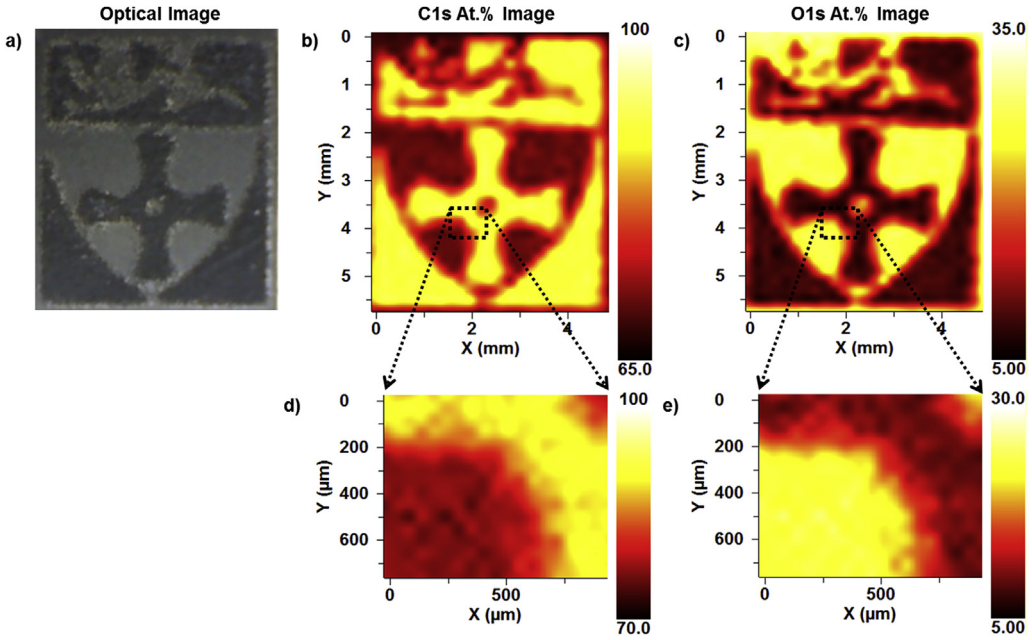

Fig. 6. Optical and XPS elemental maps of a laser-scribed pattern of reduced graphene oxide on a graphene oxide film. The pattern is the Newcastle University Shield, with (a) a photograph of the pattern, (b) and (c) XPS maps of the carbon and oxygen atomic percentages respectively, (d) and (e) higher spatial resolution maps of the highlighted areas. (A colour version of this figure can be viewed online.)

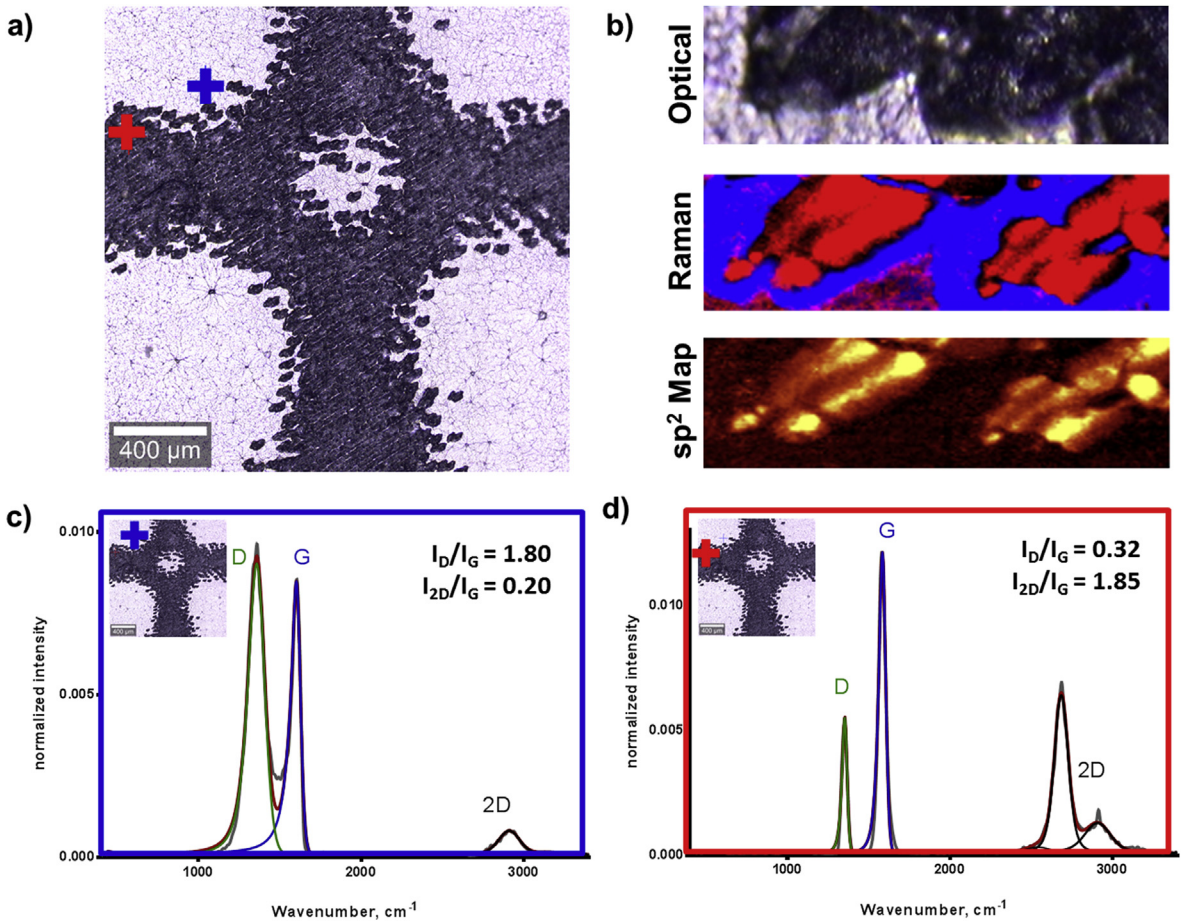

Fig. 7. Results of the Raman characterisation of the patterned GO surface. (a) The optical image from within the instrument showing the central feature on the sample, the blue and red crosses indicate regions where spectra in (c) and (d) were collected respectively. (b) Optical and Raman maps of a boundary region of the pattern showing individual laser scribed features. The red regions are those where $I_D/I_G = 0.3$, and the blue regions where $I_D/I_G = 1.8$. The sp^2 map shows regions of greatest sp^2 carbon signal. (A colour version of this figure can be viewed online.)

show an increased sp^2 carbon content. A magnified view of a boundary region between as-deposited GO and GO irradiated by individual laser pulses is presented in Fig. 7(b). Using the spectra collected from the area shown in Fig. 7(c) and (d) for as-deposited and laser-scribed respectively, a red-blue Raman intensity map could be generated using a two-component model, where the blue channel is associated with spectra similar to (c), i.e. graphene oxide-like material with intensity ratio $I_D/I_G = 1.8$, and the red channel is associated with spectra similar to (d), i.e. graphene-like material with $I_D/I_G = 0.3$.

The spectra in Fig. 7(c) and (d) of the patterned GO film indicated a clear difference in ratio of the D and G bands (I_D/I_G) for pristine and laser-scribed areas, being 1.8 and 0.3, respectively. The ratio of I_G to I_D maps extracted from multispectral imaging dataset produces an sp^2 carbon map (shown in Fig. 7(b)) with bright pixels in laser-scribed areas having higher graphitic content and darker pixels in pristine areas having decreased sp^2 character. This suggest a reduction in defect density on the graphene platelets and thus an increase in overall sp^2 character upon laser irradiation, as observed previously for similar work [22,23]. Narrowing of the D-band is observed after laser irradiation. Trusovas et al. attributed a decrease in the width of the D, G and 2D bands to an increase in order in the graphene lattice after laser irradiation with a 50 mW pulsed laser [24], experimentally very similar to the work presented here. Raman spectro-microscopy of the boundary of a laser irradiation spot on the GO shown in Fig. 7(b) gives a clear indication that the regions are different from one another. However the D-band is prominent across the surface, and the 2D band (at 2700 cm^{-1}) is weaker in intensity for laser-scribed GO than might be expected for pure graphene, and not present for the as deposited GO. The intensity of the 2D band for defective graphene structures can be associated with the level of disorder [25], so that by increasing the level of disorder, the 2D band can be absent [26]. However, its presence and/or increase after reduction is influenced by the number of layers and stacking order of the graphene sample [27]. A clear 2D peak can be distinguished for the laser-scribed GO compared to the as-deposited GO, indicative of the graphitic domain being restored in many layers (>5) [28].

Along with the elemental spectra used to generate the maps in Fig. 6, C *KLL* spectra were collected at each pixel. This allowed for MAFI maps to be generated from the D-Parameter extracted at each pixel in the XPS maps. Prior to D-Parameter analysis, spectra were processed using TFA to discard the noise from the data, providing higher quality spectra for processing. Fig. 8 shows the resulting MAFI map generated from the XPS data, with (a) generated from the 200 µm pixel spacing data and (b) from the 50 µm spacing. Here intensity in the map indicates an increase in the extracted D-Parameter, thus bright pixels are associated with regions of greater sp^2 carbon content.

Comparing the maps in Fig. 8 to those in Fig. 6, it can be concluded that the regions of greater D-Parameter and thus higher sp^2 content are associated directly with the laser-scribed regions of

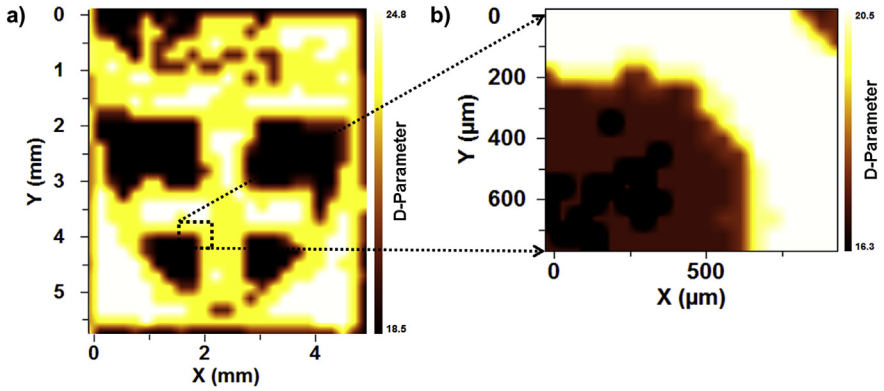

Fig. 8. MAFI images of the laser-scribed GO surface generated from data collected at the same time as Fig. 6. Intensity in these maps is now due to increases in the calculated D-Parameter, i.e. increases in sp^2 carbon content. (A colour version of this figure can be viewed online.)

the GO film. Where there remained some ambiguity in the Raman spectra due to additional effects from the number of graphene layers and the information depth of the technique, the XPS MAFI maps provide an unequivocal indication of the variation in the sp^2 content of the surface; that laser scribing results in *reduced* GO (rGO).

The MAFI image provides insight into the two predominant phases on the laser-scribed GO surface, i.e. GO and rGO, and further analysis can be performed using the MAFI image as a guide. C1s spectra were collected at every pixel, and by creating masks using the areas defined by the MAFI image average C1s spectra can be extracted for the two phases. These spectra are provided in Fig. S2, and the mask image is given in the inset. This mask was generated by creating a false-colour version of the MAFI image in CasaXPS, where red defined all areas with a D-Parameter less than 20 eV, and black defined all areas greater than 20 eV. Average spectra were then calculated in CasaXPS using the false colour image to sum the spectra within the two defined phases. While ideally the C1s peak position in XPS should give an indication of the sp^2/sp^3 content of a graphite-like surface, the laser-scribed GO surface studied here provides a case where the difference between the two is negligible, and could easily be accounted for by instrumental effects. The C *KLL* and differentiated C *KLL* spectra are presented in Fig. S3 with the extracted D-Parameter for each phase. Returning to the raw data and using the MAFI image as a guide for averaging spectra assures the analyst that the conclusions drawn from the image are robust. In this case indeed the laser-scribed GO areas had, on average, a greater D-Parameter further strengthening the assertion that the GO was reduced in the laser-scribed regions. It is worthwhile to note that the variation in the D-Parameter between the two average spectra is not as great as that observed in the MAFI image. The step size in the spectra collected at each pixel was 0.5 eV to reduce acquisition time, and thus the D-Parameter values also vary by 0.5 eV. Because the total range of D-Parameter values in the image is narrow, less than 6 eV, this results in few intensity levels and thus an appearance of significant contrast. When the average spectra are generated, the variation is measured to be much more subtle, likely an indication simply of a reasonable amount of experimental scatter between the spectra collected at each pixel.

5. Strengths and limitations of the MAFI technique

The core strength gained from combining the D-Parameter measurement with XPS imaging is the chemical specificity that results. Strong changes in carbon chemistry within the information volume of the XPS technique are unambiguously distinguished, even when the associated C1s spectra show little to no discernible difference. This results in a much more powerful imaging method when compared to images collected from the C1s region alone. Furthermore, since the D-Parameter measurement is effectively looking at the width of the Auger feature, it is completely independent of charging effects that may result from the XPS analysis. The Auger peak could shift by a number of eV in position, yet the D-Parameter measurement will remain the same. The same cannot be said when imaging using the C1s peak position, and in fact small levels of surface or differential charging will likely lead to erroneous conclusions being drawn, when one chemical state may be identified as different to another not due to their chemistry but due to differential charging between the regions at the surface. Very recently, this has been exploited by Gorham et al. to separate regions of high multi-walled carbon nanotube concentrations in an epoxy matrix [29]. However for surfaces where the different phases are still largely conductive, such as for patterned graphene oxide, the differential charging method unfortunately would not be conclusive.

MAFI is not solely applicable to XPS imaging and mapping. The *electron*-induced carbon Auger spectrum, such as that observed in Auger electron spectroscopy (AES) and scanning Auger microscopy (SAM) is just as sensitive to changes in carbon bonding as the X-ray induced feature in XPS [30]. Thus MAFI can also be applied in these complementary techniques, where significant gains can be had in spatial resolution, owing to the usage of an electron beam as the probe rather than X-rays.

A drawback to the MAFI technique is the low intensity of the C *KLL* feature relative to the C1s peak. Coupled with the already low signal that typically arises from XPS imaging/mapping techniques, long acquisition times consequently become necessary. However through the application of multivariate analysis and using the MAFI method, some gains can be made in this regard. Relatively poorer quality spectra can still ultimately result in high quality Multivariate Auger Feature Images, with clear distinction between sp^2 and sp^3 carbon on a given surface.

6. Conclusion

A method for the distinction between sp^2 and sp^3 carbon in XPS imaging through the analysis of the D-Parameter rather than the C1s peak position has been presented. From XPS images and maps collected across the X-ray induced C *KLL* Auger feature, D-Parameter values are extracted at each pixel in a stack of energy-resolved images or maps, and these values then used to generate a clear image of the sp^2 and sp^3 regions on a sample surface, the “D-

Parameter Image". Further enhancements of this technique have been made through the application of multivariate analysis in the form of Target Factor Analysis of the original spectra to de-noise the data, and improve image quality. The "Multivariate Auger Feature Imaging (MAFI)" technique provides clear identification of regions where the D-Parameter is high or low, and thus rapid and unambiguous identification of carbon in its sp^2 and sp^3 chemical states. Application of this technique to laser-scribed graphene oxides surfaces show clearly that the regions of laser irradiation resulted in a reduction of the graphene oxide platelets, and indicated by an increased D-Parameter in those regions and thus an increased sp^2 carbon content.

Acknowledgements

The authors would like to thank Dr Simon Woodman and Dr Hugo Hiden of the School of Computing Science, Newcastle University, for their invaluable input towards this work. AJB thanks Neal Fairley for many valuable conversations surrounding this work and XPS imaging using CasaXPS. This research was partially supported by U. S. Army Research Office under contract/grant number W911NF1410092, "Nanomaterials Characterisation Facility: Confocal Raman Microscope/Atomic Force Microscopy – WITec Alpha 300R". This research was supported by EPSRC grant EP/K022679/1 and the Newcastle University Digital Institute. NEXUS is an EPSRC Mid-Range Facility.

Appendix A. Supplementary data

Supplementary data related to this article can be found at http://dx.doi.org/10.1016/j.carbon.2016.05.073.

References

[1] P.K. Chu, L. Li, Characterization of amorphous and nanocrystalline carbon films, Mater. Chem. Phys. 96 (2006) 253–277, http://dx.doi.org/10.1016/j.matchemphys.2005.07.048.
[2] K.S. Novosolev, et al., A roadmap for graphene, Nature 490 (2012) 192–200, http://dx.doi.org/10.1038/nature11458.
[3] P.J. Cumpson, et al., Accurate argon cluster-ion sputter yields: measured yields and effect of the sputter threshold in practical depth-profiling by x-ray photoelectron spectroscopy and secondary ion mass spectrometry, J. Appl. Phys. 114 (2013) 124313, http://dx.doi.org/10.1063/1.4823815.
[4] P.J. Cumpson, et al., X-ray enhanced sputter rates in argon cluster ion sputter-depth profiling of polymers, J. Vac. Sci. Technol. B 31 (2013) 021208, http://dx.doi.org/10.1116/1.4793284.
[5] A.J. Barlow, et al., Observed damage during argon gas cluster depth profiles of compound semiconductors, J. Appl. Phys. 116 (2014) 054908, http://dx.doi.org/10.1063/1.4892097.
[6] A.J. Barlow, et al., Multivariate Auger Feature Imaging (MAFI) – a new approach towards chemical state identification of novel carbons in XPS imaging, Surf. Interface Anal. 47 (2015) 173–175, http://dx.doi.org/10.1002/sia.5738.
[7] P.J. Cumpson, et al., Multivariate analysis of extremely large ToFSIMS imaging datasets by a rapid PCA method, Surf. Interface Anal. 47 (2015) 986–993, http://dx.doi.org/10.1002/sia.5800.
[8] Y. Mizokawa, et al., Comparison of the C KLL first-derivative auger spectra from XPS and AES using diamond, graphite, SiC and diamond-like-carbon films, Surf. Sci. 182 (1987) 431–438, http://dx.doi.org/10.1016/0039-6028(87)90011-2.
[9] S. Kaciulis, Spectroscopy of carbon: from diamond to nitride films, Surf. Interface Anal. 44 (2012) 1155–1161, http://dx.doi.org/10.1002/sia.4892.
[10] J.C. Lascovich, R. Giorgio, S. Scaglione, Evaluation of the sp2/sp3 ratio in amorphous carbon structure by XPS and XAES, Appl. Surf. Sci. 47 (1991) 17–21, http://dx.doi.org/10.1016/0169-4332(91)90098-5.
[11] Casa Software Ltd., Teignmouth, UK. http://www.casaxps.com.
[12] J.W. Eaton, D. Bateman, S. Hauberg, R. Wehbring, GNU Octave Version 3.8.1 Manual: A High-Level Interactive Language for Numerical Computations, Createspace Independent Publishing Platform, 2014, ISBN 1441413006. http://www.gnu.org/software/octave/.
[13] K. Artyushkova, J.E. Fulghum, Identification of chemical components in XPS spectra and images using multivariate statistical analysis methods, J. Electron Spectrosc. Relat. Phenom. 121 (2001) 33–55, http://dx.doi.org/10.1016/S0368-2048(01)00325-5.
[14] K. Artyushkova, J.E. Fulghum, Multivariate image analysis methods applied to XPS imaging data sets, Surf. Interface Anal. 33 (2002) 185–195, http://dx.doi.org/10.1002/sia.1201.
[15] J. Walton, N. Fairley, Quantitative surface chemical-state microscopy by X-ray photoelectron spectroscopy, Surf. Interface Anal. 36 (2004) 89–91, http://dx.doi.org/10.1002/sia.1654.
[16] X. Zhang, et al., Graphene's potential in materials science and engineering, RSC Adv. 4 (2014) 28987–29011, http://dx.doi.org/10.1039/C4RA02817A.
[17] C.N.R. Rao, H.S.S. Ramakrishna Matte, K.S. Subrahmanyam, Synthesis and selected properties of graphene and graphene mimics, Acc. Chem. Res. 46 (2013) 149–159, http://dx.doi.org/10.1021/ar300033m.
[18] S. Stankovich, et al., Synthesis of graphene-based nanosheets via chemical reduction of exfoliated graphite oxide, Carbon 45 (2007) 1558–1565, http://dx.doi.org/10.1016/j.carbon.2007.02.034.
[19] C. Soldano, A. Mahmood, E. Dujardin, Production, properties and potential of graphene, Carbon 48 (2010) 2127–2150, http://dx.doi.org/10.1016/j.carbon.2010.01.058.
[20] E.V. Iski, et al., Graphene at the atomic-scale: synthesis, characterization, and modification, Adv. Funct. Mater. 23 (2013) 2554–2564, http://dx.doi.org/10.1002/adfm.201203421.
[21] M.F. El-Kady, R.B. Kaner, Scalable fabrication of high-power graphene micro-supercapacitors for flexible and on-chip energy storage, Nat. Commun. 4 (2013) 1475, http://dx.doi.org/10.1038/ncomms2446.
[22] M. Cheng, et al., Restoration of graphene from graphene oxide by defect repair, Carbon 50 (2012) 2581–2587, http://dx.doi.org/10.1016/j.carbon.2012.02.016.
[23] R.Y.N. Gengler, et al., Revealing the ultrafast process behind the photoreduction of graphene oxide, Nat. Commun. 4 (2013), http://dx.doi.org/10.1038/ncomms3560.
[24] R. Trusovas, et al., Reduction of graphite oxide to graphene with laser irradiation, Carbon 52 (2013) 574–582, http://dx.doi.org/10.1016/j.carbon.2012.10.017.
[25] G. Eda, G. Fanchini, M. Chhowalla, Large-area ultrathin films of reduced graphene oxide as a transparent and flexible electronic material, Nat. Nanotechnol. 3 (2008) 270–274, http://dx.doi.org/10.1038/nnano.2008.83.
[26] I. Childres, et al., Raman Spectroscopy of Graphene and Related Materials, in New Developments in Photon and Materials Research, Nova Science Publishers, 2013, ISBN 978-1-62618-384-1.
[27] A. Kaniyoor, S. Ramaprabhu, A Raman spectroscopic investigation of graphite oxide derived graphene, AIP Adv. 2 (2012) 032183, http://dx.doi.org/10.1063/1.4756995.
[28] A.C. Ferrari, D.M. Basko, Raman spectroscopy as a versatile tool for studying the properties of graphene, Nat. Nanotechnol. 8 (2013) 235–246, http://dx.doi.org/10.1038/nnano.2013.46.
[29] J.M. Gorham, et al., Detecting carbon in carbon: exploiting differential charging to obtain information on the chemical identity and spatial location of carbon nanotube aggregates in composites by imaging X-ray photoelectron spectroscopy, Carbon 96 (2015) 1208–1216, http://dx.doi.org/10.1016/j.carbon.2015.10.073.
[30] L. Lampert, et al., Towards the electron spectroscopy graphene fingerprint, Microsc. Microanal. 21 (2015) 1149–1150, http://dx.doi.org/10.1017/S1431927615006534.